Modeling of Mixed Cracks in Rock-Like Brittle Materials Under Compressive Stresses by a Double-Phase-Field Method

Zhan Yu, Yue Sun, Minh-Ngoc Vu, Jian-Fu Shao

Modelling of mixed cracks in rock-like brittle materials under compressive stresses by a double phase-field method

Zhan YU[a,b], Yue SUN[b], Minh-Ngoc VU[c], Jian-Fu SHAO[a,b,*]

[a] *Key Laboratory of Ministry of Education on Safe Mining of Deep Metal Mines, College of Resources and Civil Engineering, Northeastern University, Shenyang, 110819, China*
[b] *University of Lille, CNRS, EC Lille, LaMcube, UMR9013, 59000 Lille, France*
[c] *Andra, Chatenay Malabry, France*

Abstract

A new phase-field method is proposed in this paper for modelling complex cracking process in rock-like brittle materials under compression-dominating stresses. For this purpose, two crack fields are introduced in order to respectively describe tensile and shear cracks, related to two independent dissipation processes. The evolution of these fields is described by using the variational principle and thermodynamics framework. The proposed method is implemented in a finite element code and applied to investigating cracking process in a rock-like sample containing two initial flaws and subjected to uniaxial and bi-axial compression. Both tensile wing and shear cracks as well as crack coalescence observed in laboratory tests are successfully reproduced by the proposed method. Differently with most previous studies, the effect of confining stress on shear cracking growth is well described.

Keywords: Damage, cracking, crack coalescence, phase-field method, rock-like materials, Compressive stresses

Highlights

- A new phase-field model is developed for modeling complex cracking in rock-like materials under compressive loads.
- Two damage fields are introduced in order to describe tensile and shear cracks.

*Corresponding author: jian-fu.shao@polytech-lille.fr

- A new criterion is proposed for the description of shear crack under multi-axial compression.
- The new model is able to well reproduce complex cracking processes observed in laboratory tests.

1. Introduction

In many engineering materials, macroscopic fractures are generally generated by the coalescence of diffuse micro-cracks. The description of transition from diffuse micro-cracks to localized macroscopic fractures is the key issue of modelling failure process in materials and structures. Further, under multi-axial loading conditions, multiple fractures can initiate, propagate and interact. There is a real challenge for numerical modelling. Different methods have been developed during the last decades to deal with this complex subject. For example, enriched finite element methods have been first developed to account for displacement discontinuities along crack surfaces at the elementary level with the help of enriched shape functions [1]. Extended finite element methods (XFEM) have been developed to deal with crack displacement discontinuities by using nodal enrichment techniques [2]. These methods have successfully been applied to different types of materials and structures, in particular hydraulic fracturing in porous rocks [3, 4]. In these two types of methods, the transition from diffuse damage to localized fractures is still a pending issue. The thick level set has been recently proposed to remediate the issue of damage-fracturing transition [5, 6]. The description of multiple cracks in three-dimensional conditions is also a delicate task. On the other hand, based on homogenization techniques, some micro-mechanical models have also been developed for capturing the initiation and growth of micro-cracks and their transition to localized cracks in a representative elementary volume [7, 8, 9]. The efficiency of such models at the structure scale still needs to be demonstrated.

More recently, based on the framework of variational principle for fracture mechanics [10] and the optimal approximations methods of functionals with jumps [11, 12, 13], the so-called phase-field method has been rapidly developed [14]. The sharp topology of crack is

approximated by a regularized one which is a non-local function of damage variable and its gradient (phase-field). The phase-field is determined by a specific boundary values problem. This approach is particularly suitable to deal with the natural transition from diffuse damage to localized cracks, interacting multiple cracks and three dimensional problems. Different extensions have been proposed for various purposes, dynamic brittle fracture [15], fast computing with a new hybrid formulation [16], multi-physics problems [17], finite deformation [18], and coupling between damage and plasticity [19, 20], etc..

In most previous studies, the accent was put on tensile cracks which are driven by the elastic strain energy related to tensile eigenvalues. As in a wide range of engineering structures, shear cracks are also an important mechanism, different extensions have been proposed in some recent works. For instance in [21, 22], the authors have proposed a specific decomposition of the ratio between driving strain energy and critical fracture energy into a tensile part (mode I) and a shear part (mode II). The phase-field evolution is thus driven by both the tensile and shear strain energy. And each part is controlled by a critical fracture energy (mode I and mode II). The efficiency of this method in modelling mixed crack propagation has been demonstrated. More recently, in [23], the concept of multiple phase-field has been introduced to describe the damage accumulation in different cleavage planes of polycrystalline materials. Similarly, this type of concept has been applied to anisotropic materials in order to capture different cracking patterns in [24]. However, those previous studies have mainly focused on tensile and shear loads.

Most rock-like materials are subjected to compression-dominating stresses. Crack initiation and propagation in these materials subjected to compressive loads exhibit complex and mixed patterns [25, 26], such as compression-induced tensile wing and shear cracks. Further, the mechanical behavior of rock-like materials is strongly dependent on compressive mean stress. For instance, the shear crack growth is directly affected by the compressive normal stress. For this purpose, a phase-field model for compressive-shear fracture was proposed by introducing a hybrid approach in [27]. Moreover, based on the assumption of frictional contact [28] and friction energy [29], some authors proposed a frictional fracture phase-field model [30] and a mixed-FE scheme [31] to deal with compression-induced shear cracks in

rock-like materials. On the other hand, the phase-field model for mixed-mode fracture were introduced in [32, 33]. Further, some authors focused on the compressive-ductile behavior of mixed-mode phase-field model by considering micro-structure [34, 35].

The so-called multi phase-field were firstly proposed and applied on polycrystal [36]. The conception of "multi" is introduced to describe the anisotropy of damage on cleavage planes. The same conception is also used in the most work of multi phase-field [37, 38, 39]. Conversely, it is worth to note that the conception of the double phase-field is different from that of the multi phase-field, even if they have a similar call. The principal feature of double phase-field method is the use of two damage variables (or more than two if necessary). This conception is firstly appeared in the study of [40], the two damage variables is introduced to identify the different effect of longitudinal and transverse failure for anisotropic materials. For a different purpose, [41] proposed a double phase-field with the damage variables defined as tensile damage and shear damage, which are driven by the energy decomposed according to the strain state. Similarly, [42] proposed a double phase-field method to consider the tensile and compressive-shear crack. The onset/effect of tensile crack and compressive-shear crack are according to crack conditions of "open", "stick" and "slip". The two types of crack are identified based on a complex calculation due to the stress in the direction perpendicular and parallel to the interface of the crack.

In the present study, a new phase-field method is proposed for modelling mixed cracks in rock-like brittle materials subjected to compression-dominating stresses. Two phase-field variables are introduced to describe the tensile and compressive-shear cracks respectively. Mixed cracks can be represented by the combination of these two phase-field variables by using a spectral decomposition of stress. Different from the work of [41], the tensile and compressive crack are distinguished by stat of stress instead of strain in order to adopt the rock-like material. Furthermore, with a same purpose of [42], by using a more simply and also reasonable way, a modified Morh-Coulomb criterion is introduced to identify the compressive-shear crack, which is more suitable to consider the properties of internal friction and cohesion for rock-like material. Another way to deal with the issue of mixed crack is provided. The efficiency of the proposed method is assessed through comparisons

between numerical results and experimental evidence. It is shown that different types of crack propagation scenarios can be well described by the proposed method.

2. A double phase-field method

2.1. Regularized crack density

We consider here a solid body occupying the volume Ω, subjected to the body force $\mathbf{f}_b$ in Ω, the surface force $\mathbf{t}_N$ on its external boundary $\partial\Omega_f$ and the prescribed displacement $\overline{\mathbf{u}}$ on its external boundary $\partial\Omega_u$. Due to the applied loads, there is initiation and propagation of cracks. In the case of rock like materials under compression-dominating stresses, complex cracking processes have been observed [43, 44, 45]. In general, three types of cracks, namely tensile, shear and mixed, can initiate and propagate depending on loading path and material microstructure. Under direct tension or in triaxial extension conditions, tensile cracks represent the main process. Under triaxial compression conditions, in particular when confining stress is high, frictional shear cracks are the dominant mechanism. In general loading conditions, mixed cracks can be generated by combined tensile and shear strains or stresses. In order to conveniently describe such complex cracking processes, two independent crack fields are here introduced to respectively represent the tensile and shear cracks. Mixed cracks are then described by the combination of these two fields.

In the framework of phase-field method, the real crack surface area is approximated by the regularized one [14]. By considering the two crack fields, the total regularized crack surface area Γ_{l_d} is expressed as follows:

$$\Gamma_{l_d} = \Gamma^t_{l_d}(d^t) + \Gamma^s_{l_d}(d^s) = \int_\Omega \{\gamma^t(d^t, \nabla d^t) + \gamma^s(d^s, \nabla d^s)\} dV \tag{1}$$

where $\Gamma^\alpha_{l_d}$ $(\alpha = t, s)$ are the contributions of tensile and shear cracks to the total crack surface area. Two scalar-valued functions $\gamma^\alpha(d^\alpha, \nabla d^\alpha)$ denote the tensile and shear crack density (surface area per unit volume). There are different forms available to define the crack surface density γ^α. A common form was introduced in [11] and it is adopted here:

$$\gamma^\alpha(d^\alpha, \nabla d^\alpha) = \frac{1}{2l_d}(d^\alpha)^2 + \frac{l_d}{2}\nabla d^\alpha . \nabla d^\alpha \quad ; \quad \alpha = t, s \tag{2}$$

In these functions, a scalar-valued variable $d^\alpha(\mathbf{x})$ $(\alpha = t, s)$ is introduced for each type of crack and it is conventionally called the phase-field (or crack) variable. It is worth noticing that the crack surface density γ^α is a function of d^α and its gradient ∇d^α. l_d is a length scale parameter controlling the width of regularized smeared crack surfaces. This non-local property allows the phase-field method to avoid the pathologic mesh dependency of numerical solution. Further, the value of $d^\alpha(\mathbf{x})$ $(\alpha = t, s)$ also indicate the current damage state of material, more precisely $d^\alpha(\mathbf{x}) = 0$ being the sound state while $d^\alpha(\mathbf{x}) = 1$ the fully damaged one as shown in Figure 1.

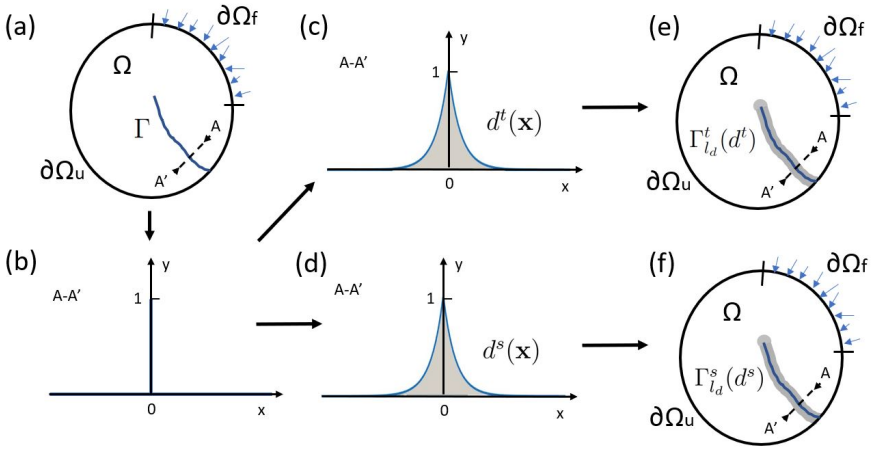

Figure 1: (a) A sharp crack Γ inside solid body Ω; (b) auxiliary damage variable in sharp crack topology along the 1D line A-A'; (c) and (d) tensile and shear crack phase-field in regularized crack topology along the 1D line A-A'; (e) and (f) regularized representation of tensile and shear cracks with equivalent crack surfaces $\Gamma(d^t)$ and $\Gamma(d^s)$

Further, according to the Griffith theory of linear fracture mechanics, the energy needed for the creation of a crack surface area is characterized by the material toughness or fracture energy. With the regularized smooth representation of cracks adopted here, one can express the energy density per unit volume needed for the creation of tensile and shear cracks as follows:

$$w_c(d^t, d^s, \nabla d^t, \nabla d^s) = g_c^t \gamma^t(d^t, \nabla d^t) + g_c^s \gamma^s(d^s, \nabla d^s) \tag{3}$$

g_c^t and g_c^s denotes the material toughness for the tensile and shear crack respectively.

2.2. Variational framework

According to the variational approach to fracture mechanics of elastic materials proposed in [10], under the isothermal conditions, the total energy functional of a solid domain Ω is composed of the elastic strain energy and that requested to create the cracks, with the regularized crack fields adopted above, one gets:

$$E(\boldsymbol{\varepsilon}, d^t, d^s) = \int_\Omega w_e(\boldsymbol{\varepsilon}, d^t, d^s) dV + \int_\Omega w_c dV \tag{4}$$

w_e is the elastic strain energy density of cracked material. $\boldsymbol{\epsilon}(\mathbf{u})$ denotes the second order linear strain tensor with $\mathbf{u}(\mathbf{x})$ being the displacement vector such as $\boldsymbol{\epsilon} = \nabla^s \mathbf{u}$.

2.2.1. Elastic strain energy

In the present study, two crack fields are introduced and affect differently the elastic strain energy. In order to better describe the coupling between the cracking processes and elastic properties of cracked material, the elastic strain energy of undamaged solid is decomposed into a tensile part $w^0_{e+}+$ and a compressive part w^0_{e-}:

$$w^0_e(\boldsymbol{\epsilon}) = w^0_{e+}(\boldsymbol{\epsilon}) + w^0_{e-}(\boldsymbol{\epsilon}) = \frac{1}{2}\boldsymbol{\sigma}^+ : \boldsymbol{\epsilon} + \frac{1}{2}\boldsymbol{\sigma}^- : \boldsymbol{\epsilon} \tag{5}$$

Two symmetric tensors $\boldsymbol{\sigma}^\pm$ denote the tensile and compressive parts of the Cauchy stress tensor $\boldsymbol{\sigma}$, and they are calculated by using the following fourth order projection operators $\mathbb{P}^\pm_\sigma$:

$$\begin{cases} \boldsymbol{\sigma}_+ = \mathbb{P}^+_\sigma : \boldsymbol{\sigma} \\ \boldsymbol{\sigma}_- = \mathbb{P}^-_\sigma : \boldsymbol{\sigma} \end{cases} \tag{6}$$

These operators are further constructed from the spectral decomposition of the stress tensor proposed in [46, 47]:

$$\begin{cases} \mathbb{P}^+_\sigma = \sum_{\beta=1}^3 \langle \sigma^\beta \rangle_+ \boldsymbol{n}^\beta \otimes \boldsymbol{n}^\beta \otimes \boldsymbol{n}^\beta \otimes \boldsymbol{n}^\beta \\ \mathbb{P}^-_\sigma = \mathbb{I} - \mathbb{P}^+_\sigma \end{cases} \tag{7}$$

$\mathbb{I}$ denotes the fourth-order identity tensor. $\boldsymbol{n}^\beta (\beta = 1, 2, 3)$ define the three orthogonal principal directions of the stress tensor while σ^β are the three principal stresses. The bracket

$\langle . \rangle_+$ is defined as:

$$\begin{cases} \langle a \rangle_+ = a, & a \geq 0 \\ \langle a \rangle_+ = 0, & a < 0 \end{cases} \tag{8}$$

It is worth noticing that the projection operators are widely used for the decomposition of stress or strain tensor into tensile and compressive parts, including some previous phase-field models [48, 49, 50]. In general, even for elastically isotropic materials, the projection operators for stress $\mathbb{P}_\sigma$ and for strain $\mathbb{P}_\epsilon$ are different. As in the previous work [50], the decomposition of stress tensor is adopted here. Compared with the strain tensor decomposition as that used in [14], the stress decomposition avoids the implication of elastic parameters. It is particularly convenient for future extension to initial anisotropic materials.

The elastic properties of cracked material are affected by the growth of cracks. This is generally described by introducing different forms of degradation functions. In the present study, two degradation functions are defined respectively for the tensile and shear cracks. The elastic strain energy of cracked material is expressed as follows:

$$w_e(\boldsymbol{\epsilon}, d^t, d^s) = h_t(d^t) w_{e+}^0 + h_s(d^s) w_{e-}^0 \tag{9}$$

The common form widely used in previous studies [48, 49, 50] is adopted here for the two degradation functions:

$$h_\alpha(d^\alpha) = (1 - d^\alpha)^2 (1 - k) + k; \quad \alpha = t, s \tag{10}$$

k is a small positive value that is used to ensure the positive definiteness of elastic stiffness tensor after the material is fully broken ($d^\alpha = 1$).

2.2.2. Governing equations of crack fields

Based on the expressions of w_e and w_c defined above, the total energy functional E can be detailed in the following form:

$$\begin{aligned} E &= \int_\Omega w_e(\boldsymbol{\varepsilon}, d^t, d^s) dV + \int_\Omega w_c(d^t, d^s, \nabla d^t, \nabla d^s) dV \\ &= \int_\Omega \left\{ h_t(d^t) w_{e+}^0 + h_s(d^s) w_{e-}^0 \right\} dV + \int_\Omega \left\{ g_c^t \gamma^t(d^t, \nabla d^t) + g_c^s \gamma^s(d^s, \nabla d^s) \right\} dV \end{aligned} \tag{11}$$

We assume that the growths of tensile and shear cracks are two independent dissipation processes. Each of them verifies the positiveness condition independently. Further, inspired by the previous studies [51, 52], each crack field can be determined by solving the minimization problem of the energy functional E. By calculating the first order variation of E and using the unilateral stationary condition for the total energy functional with respect to each crack variable, namely $\delta E = 0$ for $\delta d^\alpha > 0$ and $\delta E > 0$ for $\delta d^\alpha = 0$ ($\alpha = t, s$), the following governing equations for the evolution of two crack fields ($\alpha = t, s$) can be derived:

$$\begin{cases} -\frac{\partial w_e}{\partial d^\alpha} - g_c^\alpha \delta_{d^\alpha}\gamma^\alpha = 0 \quad , \quad \dot{d^\alpha} > 0 \quad , \quad \text{in} \quad \Omega \\ -\frac{\partial w_e}{\partial d^\alpha} - g_c^\alpha \delta_{d^\alpha}\gamma^\alpha \leq 0 \quad , \quad \dot{d^\alpha} = 0 \quad , \quad \text{in} \quad \Omega \\ \frac{\partial \gamma}{\partial \boldsymbol{\nabla} d^\alpha}.\mathbf{n} = 0 \quad , \quad \text{on} \quad \delta\Omega \end{cases} \tag{12}$$

where $\delta_{d^\alpha}\gamma^\alpha = \dfrac{\partial \gamma^\alpha}{\partial d^\alpha} - div\left(\frac{\partial \gamma^\alpha}{\partial \boldsymbol{\nabla} d^\alpha}\right)$ denotes the variational derivative of crack field d^α [51, 52]. By substituting w_e and γ^α by their specific forms presented above, one obtains the governing equations for two crack fields as follows:

$$\begin{cases} -h_t'(d^t) w_{e+}^0 - g_c^t \left\{ \frac{1}{l_d} d^t - l_d div(\boldsymbol{\nabla} d^t) \right\} = 0 \quad , \quad \dot{d^t} > 0 \\ -h_s'(d^s) w_{e-}^0 - g_c^s \left\{ \frac{1}{l_d} d^s - l_d div(\boldsymbol{\nabla} d^s) \right\} = 0 \quad , \quad \dot{d^s} > 0 \end{cases} \tag{13}$$

where $h_t'(d^t) = -2(1-k)(1-d^t)$ and $h_s'(d^s) = -2(1-k)(1-d^s)$ are the derivatives of two degradation functions with respect to two damage variables.

From the threshold function (13)(b), it is observed that the evolution of the shear crack d^s is driven by the compressive part of the elastic strain energy associated with the intact state w_{e-}^0. This is physically not fully justified. In practice, for most rock-like materials under compressive stresses, the shear crack is physically controlled by a generalized shear stress. The later can be well represented by the shear force defined by the widely used Mohr-Coulomb criterion. Based on this physical background and inspired by some previous studies [53, 27], an alternative driving energy w^s is defined as follows for the description of shear crack growth:

$$w^s(\boldsymbol{\sigma}) = \frac{1}{2G}\left\langle \frac{\sigma_1 - \sigma_3}{2cos\varphi} + \frac{\sigma_1 + \sigma_3}{2} tan\varphi - c \right\rangle_+^2 \tag{14}$$

In this relation, σ_1 and σ_3 are the major and minor principal stress respectively. G is the initial shear modulus of intact material. φ denotes the internal friction angle and c the cohesion. Moreover, it is assumed that the shear crack growth occurs only in the compressive domain of principal stresses. Therefore, the driving energy of shear crack growth corresponds to the compressive part of w^s, which is defined as:

$$w^s_-(\boldsymbol{\sigma}^-) = \frac{1}{2G}\Big\langle \frac{\langle\sigma_1\rangle_- - \langle\sigma_3\rangle_-}{2cos\varphi} + \frac{\langle\sigma_1\rangle_- + \langle\sigma_3\rangle_-}{2} tan\varphi - c \Big\rangle^2_+ \tag{15}$$

with the bracket $\langle . \rangle_-$ defining:

$$\begin{cases} \langle a\rangle_- = 0, & a \geq 0 \\ \langle a\rangle_- = a, & a < 0 \end{cases} \tag{16}$$

By substituting the physically-based driving energy for the compressive shear crack growth for (13), the new criteria for two crack fields is expressed as:

$$\begin{cases} -h'_t(d^t) w^0_{e+} - g^t_c \left\{ \frac{1}{l_d} d^t - l_d div(\boldsymbol{\nabla} d^t) \right\} = 0 \quad , \quad \dot{d}^t > 0 \\ -h'_s(d^s) w^s_- - g^s_c \left\{ \frac{1}{l_d} d^s - l_d div(\boldsymbol{\nabla} d^s) \right\} = 0 \quad , \quad \dot{d}^s > 0 \end{cases} \tag{17}$$

On the other hand, in order to describe the irreversible process of crack growth in general loading paths with unloading and reloading cycles, the concept of loading history functional has been introduced in [54]. Based on that concept, two energy history functionals are here defined as follows for the grow description of tensile and shear cracks:

$$\begin{cases} \mathcal{H}^t = max[w^0_{e+}(\boldsymbol{\sigma}^+, \tau)]_{\tau\in[0,t]} \\ \mathcal{H}^s_- = max[w^s_-(\boldsymbol{\sigma}^-, \tau)]_{\tau\in[0,t]} \end{cases} \tag{18}$$

The time variable τ designates the loading history from the initial state to the current time step t. Using these energy history functionals, the evolution of the tensile and shear crack is determined by the following criteria:

$$\begin{cases} -h'_t(d^t) \mathcal{H}^t - g^t_c \left\{ \frac{1}{l_d} d^t - l_d div(\boldsymbol{\nabla} d^t) \right\} = 0 \\ -h'_s(d^s) \mathcal{H}^s_- - g^s_c \left\{ \frac{1}{l_d} d^s - l_d div(\boldsymbol{\nabla} d^s) \right\} = 0 \end{cases} \tag{19}$$

3. Numerical implementation with finite element method

The problem to be solved here consists in the determination of displacement field $\mathbf{u}(\mathbf{x})$, the tensile crack field $d^t(\mathbf{x})$ and the shear crack field $d^s(\mathbf{x})$, at each loading step and with the boundary conditions defined above. For this purpose, the total potential energy is expressed as:

$$\Pi = E(\mathbf{u}, d^t, d^s) - \int_\Omega \mathbf{f}_b \cdot \mathbf{u} d\Omega - \int_{\partial\Omega_f} \mathbf{t}_N \cdot \mathbf{u} dA \tag{20}$$

The stationarity condition of the potential energy $\delta\Pi = 0$ leads to three coupled systems of equations to be solved in terms of the displacement, the tensile crack and the shear crack fields respectively. However, due to the growth of cracks, it is needed to solve a strongly non-linear problem. For this purpose, the whole loading path is divided into a number of increments or time steps. Starting from the initial known values of all physical quantities, at the end of loading step i, the values of $\mathbf{u}(\mathbf{x}, t_i)$, $d^t(\mathbf{x}, t_i)$ and $d^s(\mathbf{x}, t_i)$ are assumed to be known. During the loading step $t_{t+1} = t_i + \Delta t_{t+1}$, the solutions to be determined are the increments of three principal unknowns, namely $\Delta\mathbf{u}(\mathbf{x}, \Delta t_{t+1})$, $\Delta d^t(\mathbf{x}, \Delta t_{t+1})$ and $\Delta d^s(\mathbf{x}, \Delta t_{t+1})$.

The finite element method is adopted in the present work. Based on the geometrical discretization and with the help of the shape functions and their derivatives for the type of element adopted, one obtains three discrete systems of equations to be solved.

For the mechanical problem, the Cauchy stress tensor $\boldsymbol{\sigma}$ verifies the following equilibrium equations:

$$\begin{cases} \nabla \cdot \boldsymbol{\sigma} + \mathbf{f}_b = 0 \quad \text{in } \Omega \\ \boldsymbol{\sigma} \cdot \mathbf{n} = \mathbf{t}_N \quad \text{on } \partial\Omega_t \end{cases} \tag{21}$$

The constitutive relation of cracked material is defined by:

$$\boldsymbol{\sigma} = \mathbb{C}(d^t, d^s) : \boldsymbol{\epsilon} \;\; ; \;\; \mathbb{C}(d^t, d^s) = h_t(d^t)\mathbb{P}_\sigma^+ : \mathbb{C}^0 + h_s(d^s)\mathbb{P}_\sigma^- : \mathbb{C}^0 \tag{22}$$

where $\mathbb{C}^0$ is the elastic stiffness matrix of intact material. Together with the kinematic relation $\boldsymbol{\epsilon} = \nabla^s\mathbf{u}$, the discrete system of equations of the mechanical problem is given by:

$$\begin{cases} \mathbf{K}^u \triangle\mathbf{U} = \triangle\mathbf{F} \\ \mathbf{K}^u = \int_\Omega \mathbf{B}_u^T \mathbb{C} \mathbf{B}_u d\Omega \\ \triangle\mathbf{F} = \int_\Omega \mathbf{N}_u^T \triangle\mathbf{f}_b d\Omega + \int_{\partial\Omega_f} \mathbf{N}_u^T \triangle\mathbf{t}_N dA \end{cases} \tag{23}$$

$\mathbf{N}_u$ and $\mathbf{B}_u$ are respectively the matrix of shape functions and related derivatives of displacement components. $\mathbf{K}^u$ is the global stiffness matrix. $\triangle\mathbf{U}$ and $\triangle\mathbf{F}$ denote the column matrices of increment nodal displacements and forces during the current loading step (for the sake of simplicity, the step index $i+1$ is here omitted).

On the other hand, with the crack growth criteria (19) in hand, the tensile crack phase-field is determined by the following local equations:

$$\begin{cases} h_t'(d^t)\mathcal{H}^t + g_c^t\left\{\frac{1}{l_d}d^t - l_d div(\boldsymbol{\nabla} d^t)\right\} = 0 \quad \text{in } \Omega \\ \dot{d}^t \geq 0 \quad \text{in } \Omega \\ d^t = 1 \quad \text{on } \Gamma^t \\ \nabla d^t \cdot \mathbf{n} = 0 \quad \text{on } \partial\Omega \end{cases} \tag{24}$$

while the shear crack phase-field is described by the following ones:

$$\begin{cases} h_s'(d^s)\mathcal{H}_-^s + g_c^s\left\{\frac{1}{l_d}d^s - l_d div(\boldsymbol{\nabla} d^s)\right\} = 0 \quad \text{in } \Omega \\ \dot{d}^s \geq 0 \quad \text{in } \Omega \\ d^s = 1 \quad \text{on } \Gamma^s \\ \nabla d^s \cdot \mathbf{n} = 0 \quad \text{on } \partial\Omega \end{cases} \tag{25}$$

The same geometrical mesh is used for the phase-field problems as for the mechanical one. Further, as for the displacement field, the two crack fields and their gradients inside each element are also approximated in terms of by the nodal values by using appropriate shape functions and related derivatives. With such approximations, the following discrete systems of equations are obtained for each crack phase-field. Namely, for the tensile cracks field, one gets:

$$\begin{cases} \mathbf{K}^{d^t}\mathbf{d}^t = \mathbf{F}^{d^t} \\ \mathbf{K}^{d^t} = \int_\Omega \{(g_c^t/l_d + 2\mathcal{H}^t)\mathbf{N}_d^T\mathbf{N}_d + g_c^t l_d \mathbf{B}_d^T\mathbf{B}_d\} d\Omega \\ \mathbf{F}^{d^t} = \int_\Omega 2\mathcal{H}^t\mathbf{N}_d^T d\Omega \end{cases} \tag{26}$$

and for the shear crack field:

$$\begin{cases} \mathbf{K}^{d^s}\mathbf{d}^s = \mathbf{F}^{d^s} \\ \mathbf{K}^{d^s} = \int_\Omega \{(g_c^s/l_d + 2\mathcal{H}_-^s)\mathbf{N}_d^T\mathbf{N}_d + g_c^s l_d \mathbf{B}_d^T\mathbf{B}_d\} d\Omega \\ \mathbf{F}^{d^s} = \int_\Omega 2\mathcal{H}_-^s\mathbf{N}_d^T d\Omega \end{cases} \tag{27}$$

$\mathbf{N}_d$ and $\mathbf{B}_d$ are the matrices of shape functions and related derivatives for the approximation of two crack phase-fields. $\mathbf{K}^{d^\alpha}$ $(\alpha = t, s)$ is the global stiffness matrix related to the tensile or shear crack field. $\mathbf{F}^{d^\alpha}$ denotes the column matrix of nodal forces while $\mathbf{d}^\alpha$ that of nodal damage variables at the current loading step (for the sake of simplicity, the step index $i+1$ is here omitted). It is worth noticing that with the help of two energy history functionals defined in (18), the values of damage variables at the current loading step are directly determined as functions of the accumulated driving energy for each cracking mechanisms.

It is obvious that three fields are strongly coupled. The calculation of displacement field is influenced by the crack phase-fields due to the fact that the elastic stiffness matrix of cracked material $\mathbb{C}(\mathbf{x})$ is a function of two crack fields $d^t(\mathbf{x})$ and $d^s(\mathbf{x})$. Inversely, the growth of both tensile and shear cracks is controlled by the mechanical energy which is related to the variation of displacement field.

In this way, the so-called Alternate Minimization (AM) solver proposed in [13, 55] is used in this work because of its good robustness performance. At the iteration $k+1$ of the loading step $n+1$, two solution stages are summarized as:

Stage 1:

$$\mathbf{K}^u(\mathbb{C})\triangle\mathbf{U}_{n+1}^{k+1} = \triangle\mathbf{F}_{n+1},\ with\ \mathbb{C} = \mathbb{C}([d^t, d^s]_{n+1}^k) \tag{28}$$

-Solving the displacement $\triangle\mathbf{U}_{n+1}^{k+1}$ by using the damage values fixed $[d^t, d^s]_{n+1}^k$ obtained from the last iteration k.

Stage 2:

$$\begin{cases} \mathbf{K}^{d^t}(\mathcal{H}^t)[\mathbf{d}^t]_{n+1}^{k+1} = \mathbf{F}^{d^t}(\mathcal{H}^t),\ with\ \mathcal{H}^t = \mathcal{H}^t(U_{n+1}^{k+1}) \\ \mathbf{K}^{d^s}(\mathcal{H}_-^s)[\mathbf{d}^s]_{n+1}^{k+1} = \mathbf{F}^{d^s}(\mathcal{H}_-^s),\ with\ \mathcal{H}_-^s = \mathcal{H}_-^s(U_{n+1}^{k+1}) \end{cases} \tag{29}$$

-Solving the damage values $[d^t, d^s]_{n+1}^{k+1}$ by using the updated displacement $\mathbf{U}_{n+1}^{k+1}$ obtained from the same iteration.

The two steps are repeated until the condition $\parallel max([d^t]_{n+1}^{k+1} - [d^t]_{n+1}^k, [d^s]_{n+1}^{k+1} - [d^s]_{n+1}^k) \parallel \leq R$ is satisfied, with $R = 1 \times 10^{-5}$ being used in this work.

4. Experimental verification

In this section, the efficiency of the proposed double phase-field method, in particular its capability to describe complex cracking patterns under compression-dominating loads is verified, through the comparison between numerical results and experimental observations.

4.1. Uniaxial compression of a plate with two inclined flaws

In this example, a representative laboratory test is investigated. Uniaxial compression is performed on a rectangular thin plate containing two initial inclined flaws, as illustrated in Figure 2. Different configurations of the initial flaws can be considered. More details about the testing procedures can be found in [56, 57]. This type of test is particularly relevant for the characterization of complex failure process in brittle materials, including tensile, shear and mixed cracks and their bridging. The proposed double phase-field method is now applied to capturing such cracking patterns.

The geometry of the plate and the prescribed boundary conditions are presented in Figure 2. The length of two initial flaws is 2a=12.7mm and their width is 0.1mm. The configuration of two flaws is defined in terms of the combination "flaw angle-spacing-continuity". For example, the case of "45-a-2a" corresponds to the configuration of two flaws inclined with an angle of $\alpha = 45°$, spaced by $s = a$ and $c = 2a$. In this study, three configurations are considered, namely "45-0-2a", "45-a-2a" and "45-2a-2a" are selected for simulation. The values of mechanical parameters involved on the proposed model are selected mainly from previous studies [56, 57]. The set of values is given in Table 1. Therefor, l_d is assumed as a pure numerical parameter of the regularized model of brittle fracture which depends on element size h: $h < l_d/2$ [54]. In this work, we define $l_d = 2.5h$ for both of the tensile and shear damage field. h_r is the size of the refined element which are assigned to the region expected to have the propagation of cracks for the sake of computational efficiency. Following the study of [58], g_c^t/l_d is considered as a real material parameter, which depends on stiffness and strength: $\sigma_c = \frac{3}{16}\sqrt{\frac{3}{2}}\sqrt{\frac{Eg_c^t}{l_d}}$. g_c^s is calibrated according to the calculated toughness value of tensile crack: g_c^s=$5g_c^t$.

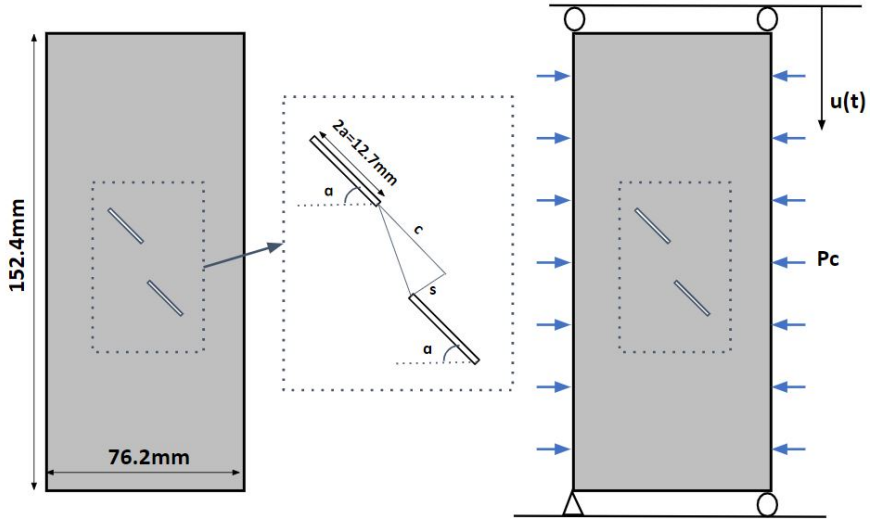

Figure 2: Geometry of plate, configuration of initial flaws and boundary conditions for uniaxial ($P_c = 0$) and bi-axial compression tests ($P_c = 7.5MPa$)

Table 1: Parameter values used in simulations of two inclined flaws test

Elastic parameters:	
E (GPa)	5.96
ν (-)	0.24
Crack fields parameters:	
σ_c(MPa)	3.2
φ (°)	30
c (MPa)	1
g_c^t (kN/mm)	4.2×10^{-6}
g_c^s (kN/mm)	21×10^{-6}
l_d (mm)	0.25
k (-)	1×10^{-9}
Mesh:	
h_r (mm)	0.1
Element number	Around 300,000
Node number	Around 300,000
Displacement increment:	
Δu (mm)	1×10^{-3}

In Figure 3, one shows the distributions of tensile and shear damage (d^t and d^s) for the case of "45-0-2a" at six subsequent values of prescribed axial displacement. The red color shows the tensile crack and the blue color shows the shear one. In order to investigate the cracking patterns more clearly, only the crack with the damage value higher than 0.5 is shown. Further, for the purpose of comparison, the main crack patterns observed in the laboratory test and reported in [56, 57] are illustrated in the same Figure. It is seen that from loading step (a) to (b), two external wing cracks and two internal wing cracks are generated from the ends of the initial flaws and they propagate towards the axial compression direction. These wing cracks are all induced by the tensile damage. At the loading step (c) and (d),

the wing cracks continue propagating in the axial direction while one shear damage band is generated from the two internal ends of the initial flaws. With the increasing of compression up to step (e) and (f), two external shear cracks are created from the two external ends of the initial flaws. And the internal shear damage band induces a sharp mixed crack which is located at the same position. All these features obtained from the numerical results match very well the experimental evidence.

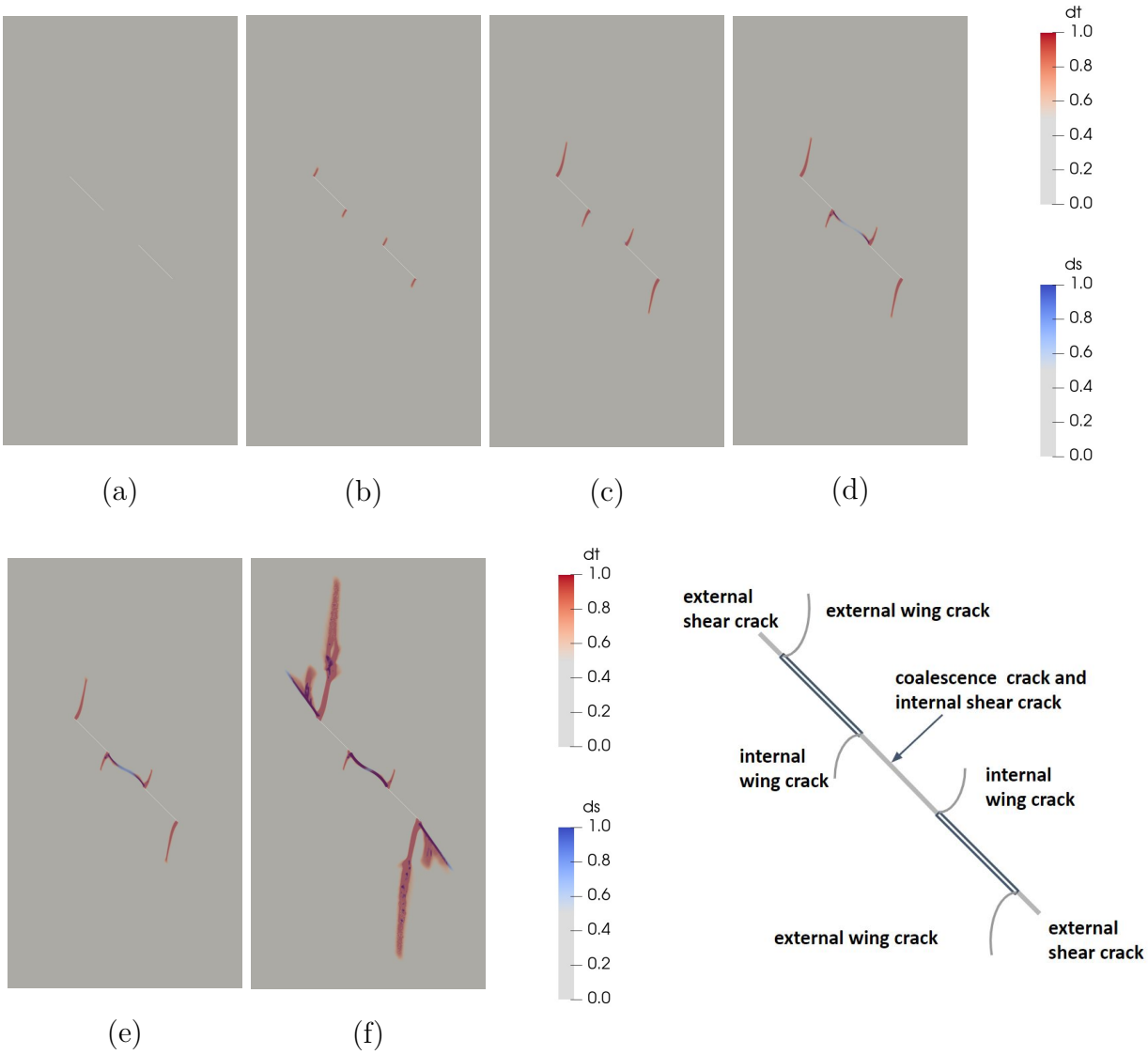

Figure 3: Distribution of tensile and shear damage for the configuration 45-0-2a at three subsequent values of axial displacement (a) u = 0 mm; (b) u = 0.620 mm; (c) u = 0.633 mm; (d) u = 0.635 mm; (e) u = 0.30 mm; (f) u = 0.666 mm

The results for the case of "45-a-2a" are presented in Figure 4. Four tensile wing cracks appear from the ends of initial flaws and propagate steadily toward the axial direction with the increase of compression. The shear cracks are also generated from the external and internal ends of initial flaws, but they propagate almost along the prolongation direction of the initial flaws. Due to the fact that the two initial flaws are not aligned ($s = 2a$), the two

internal shear cracks cannot connect each other along a straight line. As a consequence, the coalescence between the tips of two internal shear cracks emerges along a curved path by the generation of a mixed crack which propagates towards the axial compression direction. Again, all these complex cracking patterns observed in the laboratory test are well captured by the double phase-field model.

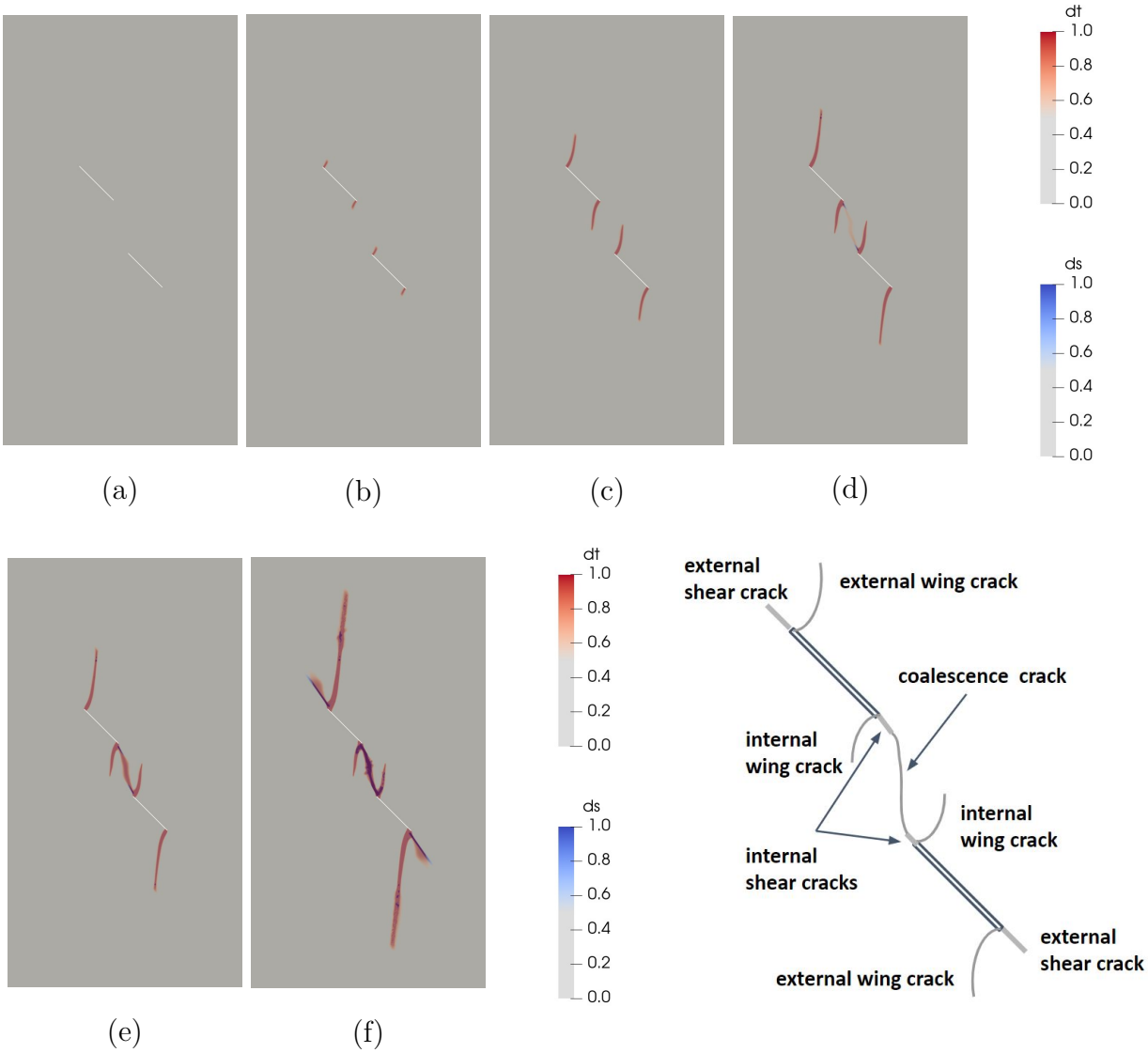

Figure 4: Distribution of tensile and shear damage variable for the case of 45-a-2a at three subsequent values of axial displacement (a) u = 0 mm; (b) u = 0.352 mm; (c) u = 0.574 mm; (d) u = 0.620 mm; (e) u = 0.623 mm; (f) u = 0.653 mm

The third configuration of two initial flaws corresponds to "45-2a-2a". The distributions of tensile and shear damage obtained are presented in Figure 5 also for three subsequent values of axial displacement. From step (a) to (b), similarly to the two previous cases, four tensile wing cracks are created and they propagate toward the compression axis. But from step (c), the two internal wing cracks have a longer propagation length than the previous configurations due to the larger spacing between the two initial flaws. At the same time, four shear cracks are also generated respectively from the ends of initial flaws. When the prescribed displacement reaches step (f), a coalescence zone is formed by the two internal wing cracks and two internal shear cracks. Once again, these complex cracking patterns are well reproduced by the proposed numerical model.

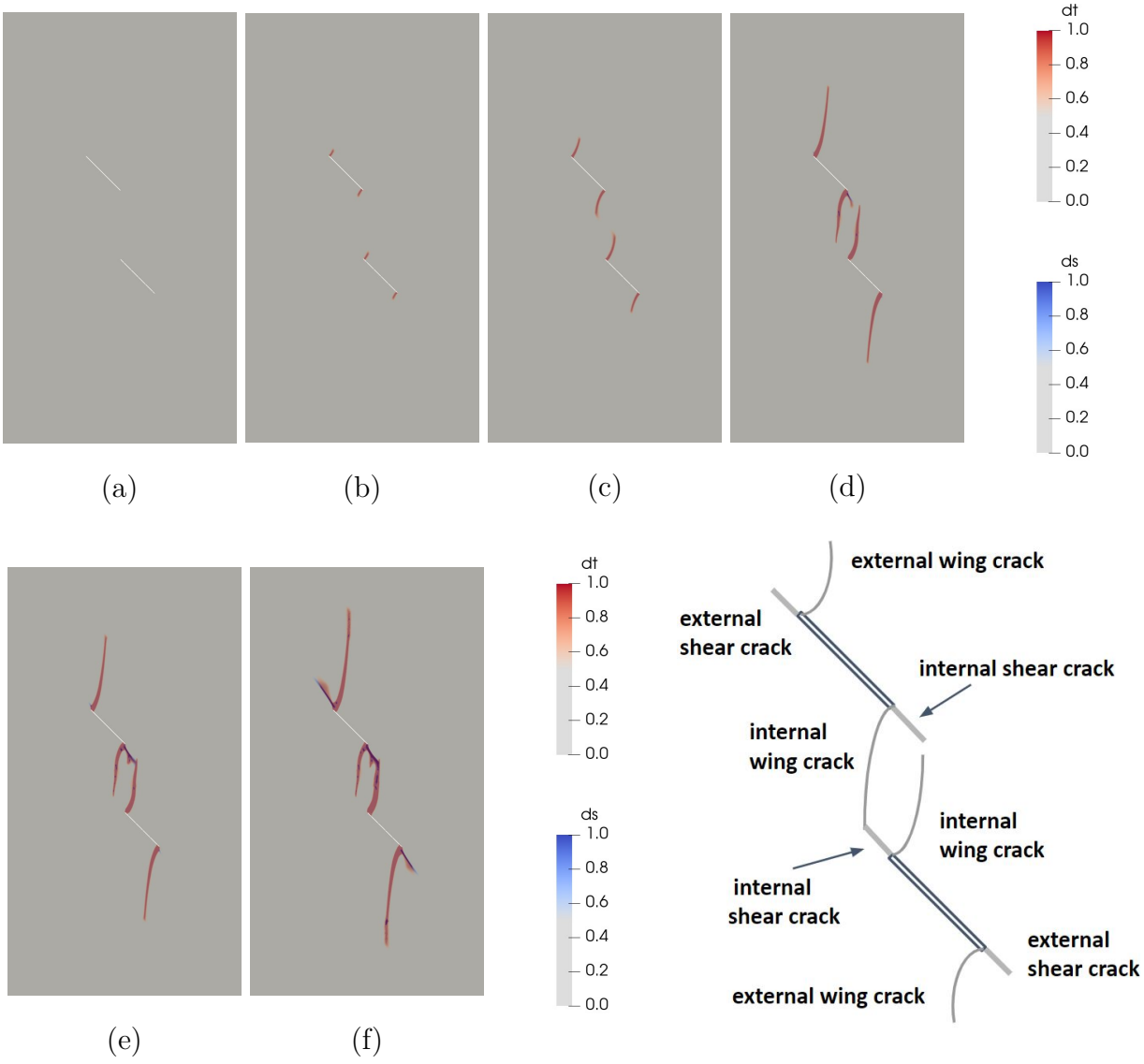

Figure 5: Distributions of tensile and shear damage for the configuration of 45-2a-2a at three subsequent steps of axial displacement (a) u = 0 mm; (b) u = 0.370 mm; (c) u = 0.561 mm; (d) u = 0.679 mm; (e) u = 0.685 mm; (f) u = 0.705 mm

In order to compare with the stress value measured from experiment and identify the stat of displacement loading in the simulation, the stress-displacement curve is given in Figure 6. Furthermore, a quantitative comparison between numerical and experimental results is provided for all of the three tests. The step (b) of Figure 3, 4 and 5 shows the moment of wing crack's onset, and the step (e) shows the one of coalescence crack's onset. Good agreement

is achieved from the quantitative comparison for both of wing crack and coalescence crack. Moreover, it is clear to see that the onset of wing crack does not affect the linear behavior of stress-displacement curves. On the other hand, the onset of coalescence crack between two initial flaws directly leads to the reduction of stress. This reasonable feature verifies the proposed double phase-field model as well.

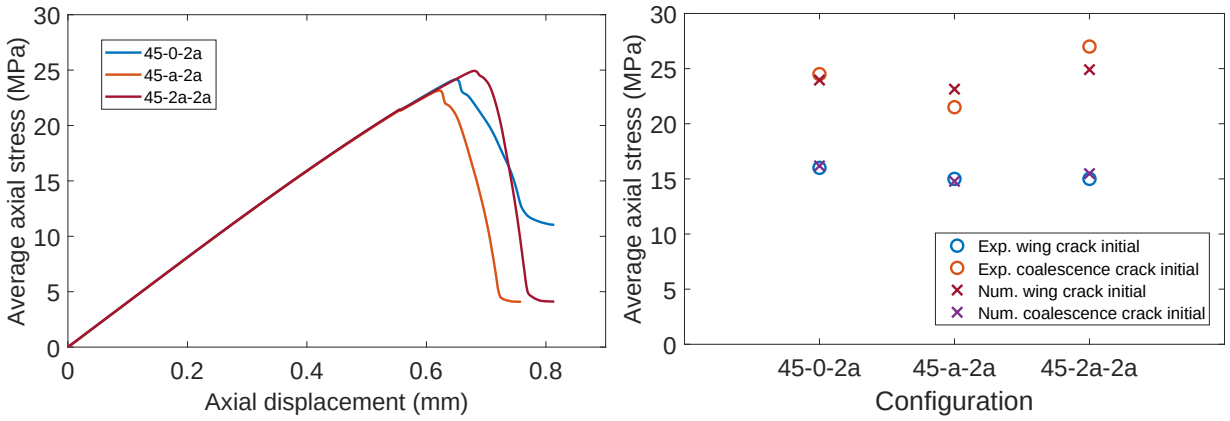

Figure 6: Left: Curves of stress-displacement for numerical test of '45-0-2a', '45-a-2a' and '45-2a-2a'; Right: The comparisons between numerical and experimental results for the wing crack and the coalescence crack initial stress

4.2. Bi-axial compression of a plate with two inclined flaws

In most previous studies devoted to rock-like materials, only uniaxial compression was generally considered. In practice, these materials are subjected to multi-axial stresses. In this study, the cracking process is investigated in a plate with two initial flaws subjected to bi-axial compression, as shown in Figure 2. Again based on the laboratory tests reported in [56, 57], the configuration "45-a-a" is here considered as an example.

In Figure 7, the distributions of tensile and shear damage are presented for six different values of axial displacement in a bi-axial compression test with a lateral stress of 7.5 MPa. It is clear that contrary to the uniaxial compression tests considered above, due to the confining effect of lateral stress, the tensile damage is significantly attenuated. The shear cracking is the principal mechanism of damage. The shear crack constitutes the bridge linking two initial flaws. Two second shear cracks are also observed around the external ends of the

initial flaws. The cracking patterns provided by the proposed phase-field method agree well with the experimental observations. It seems that the new model is able to describe the effect of confining stress on the kinetics of shear cracks commonly observed in rock-like materials.

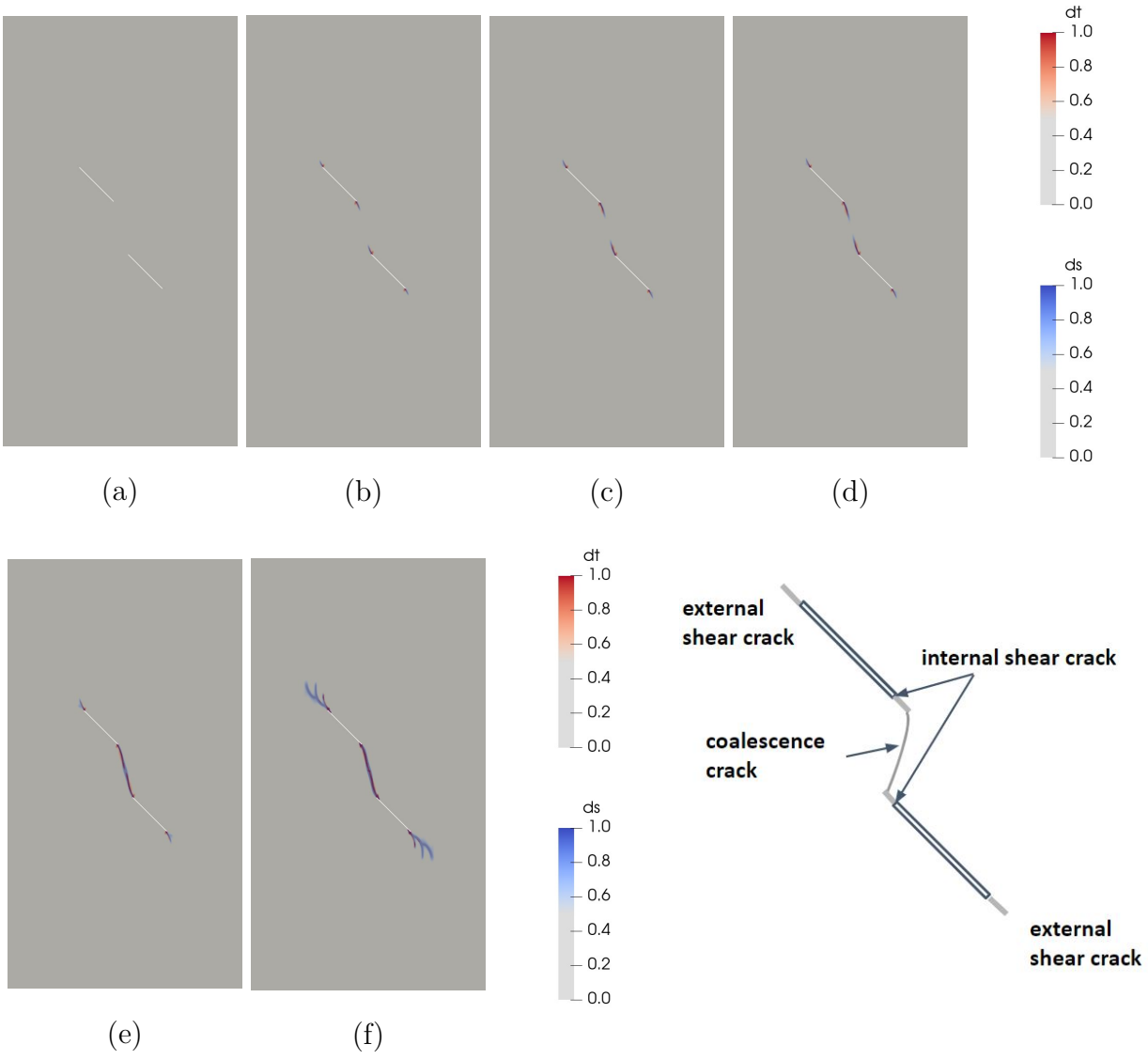

Figure 7: Distribution of tensile and shear damage for the configuration 45-a-a at three values of prescribed axial displacement at (a) u = 0 mm; (b) u = 0.793 mm; (c) u = 0.801 mm; (d) u = 0.803 mm; (e) u = 0.809 mm; (f) u = 0.850 mm, in a bi-axial compression with a lateral stress of P_c=7.5 MPa

The stress-displacement curve for the simulation of bi-axial compression is given in Figure

8.An obvious difference between the numerical and experimental results if the friction angle $\varphi = 30°$ is used as in the uniaxial compression tests. In this way, the friction angle is assumed to be increased according to the lateral stress. The simulations by using $\varphi = 32°$ and $34°$ are given. The quantitative stress result is improved while the crack model is not changed (compare with figure 7).

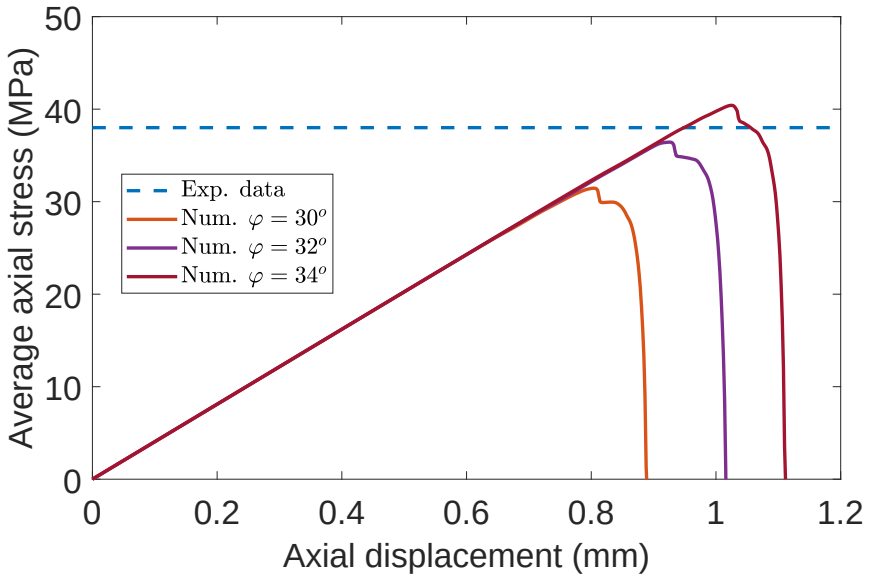

Figure 8: The curves of stress-displacement simulated by using different friction angle $\varphi = 30°$, $32°$ and $34°$ comparing with the experimental coalescence crack initial stress, in a bi-axial compression with a lateral stress of P_c=7.5 MPa

5. Discussion

The fundamental idea of this double phase-field model is proposed in order to identify the mixed crack problem from the in-situ experiment in the context of radioactive waste disposal. Since the complex damage zone due to the excavation plays an important role on the later thermo-hydromechanical coupling behavior, the concept of our double phase-field model is proposed to distinguish the tensile and compressive-shear damage in [41].
Recently, Fei and Choo[30] did a excellent work by using a similar concept of double phase-field model. Following their old work[28], they identify the crack condition as: open, stick and slip according to the direction of crack interface. The tensile and compressive-shear

crack are properly distinguished with the help of the sign of normal stress and slip criterion of crack. Comparing with the work of Fei and Choo, this work focus on the rock-like material, so that the Mohr-Coulomb criterion is modified to identify the driving force of compressive-shear crack. In this way, the further assumptions of friction crack based on Mohr-Coulomb criterion can be considered in the future study of mixed crack. On the other hand, the tensile and compressive-shear crack can exist at the same time according to the degradation of the stiffness matrix with the help of spectral decomposition. Therefore, both of two double phase-field models work well for the identification of mixed cracks by using several damage variables, but under different physical assumptions, especially for the friction crack.

6. Conclusion

In this paper, a new phase-field method has been developed for modelling complex cracking modes in rock-like brittle materials subjected to compression-dominating loads. Two interacting crack fields have been introduced for capturing the tensile and shear crack respectively. The emphasis was put on the description of shear crack growth and propagation under compressive stresses through a specific Mohr-Coulomb type frictional sliding criterion. The combination of two crack fields allows modelling mixed cracking patterns. The proposed method has been implemented in a computer code with the finite element method. It has been applied to describe complex cracking processes in brittle materials under both uniaxial and bi-axial compressive stresses. It was found that the new double phase-field method was able to capture well the main cracking features observed in laboratory tests. Furthermore, the loading stress state corresponding to the initial wing cracks and coalescence cracks is well reproduced. Compared with most previous studies, the new phase-field method is able to well describe the effect of confining stress on the growth of shear cracks commonly observed in rock-like materials. The proposed method can be easily extended to materials with an initial anisotropy and to include plastic deformation.

Acknowledgement:

This work has been partially supported by the French National Agency for radioactive waste management (ANDRA).

References

[1] J. Oliver, Modelling strong discontinuities in solid mechanics via strain softening constitutive equations, part 1: fundamentales, Internat. J. Numer. Methods Engrg. 39 (1996) 3575–3600.

[2] N. Moes, J. Dolbow, T. Belytschko, A finite element method for crack growth without remeshing, Internat. J. Numer. Methods Engrg. 46 (1999) 131–150.

[3] Q. Zeng, J. Yao, S. JF, Numerical study of hydraulic fracture propagation accounting for rock anisotropy, Journal of Petroleum Science and Engineering 160 (2018) 422–432.

[4] Q. Zeng, J. Yao, S. JF, Study of hydraulic fracturing in an anisotropic poroelastic medium via a hybrid edfm-xfem approach, Computers and Geotechnics 105 (2019) 51–68.

[5] N. Moes, C. Stolz, N. Chevaugeon, P. E. Bernard, A level set based model for damage growth: The thick level set approach, International Journal for Numerical Methods in Engineering 86 (2010) 358–380.

[6] P. E. Bernard, N. Moes, N. Chevaugeon, Damage growth modeling using the thick level set (tls) approach: Efficient discretization for quasi-static loadings, Computer Methods in Applied Mechanics and Engineering 233-236 (2012) 11–27.

[7] Q. Zhu, L. Zhao, J. Shao, Analytical and numerical analysis of frictional damage in quasi brittle materials, Journal of the Mechanics and Physics of Solids 92 (2016) 137–163.

[8] L. Zhao, Q. Zhu, J. Shao, A micromechanics-based plastic damage model for quasi brittle materials under a large range of compressive stress, International Journal of Plasticity 100 (2018) 156–176.

[9] L. Zhao, J. Shao, Q. Zhu, Analysis of localized cracking in quasi-brittle materials with a micromechanics based friction damage approach, Journal of the Mechanics and Physics of Solids 119 (2018) 163–187.

[10] G. A. Francfort, J.-J. Marigo, Revisiting brittle fracture as an energy minimization problem, Journal of the Mechanics and Physics of Solids 46 (8) (1998) 1319–1342.

[11] L. Ambrosio, V. M. Tortorelli, Approximation of functional depending on jumps by elliptic functional via t-convergence, Communications on Pure and Applied Mathematics 43 (8) (1990) 999–1036.

[12] D. Mumford, J. Shah, Optimal approximations by piecewise smooth functions and associated variational problems, Communications on pure and applied mathematics 42 (5) (1989) 577–685.

[13] B. Bourdin, G. A. Francfort, J.-J. Marigo, Numerical experiments in revisited brittle fracture, Journal of the Mechanics and Physics of Solids 48 (4) (2000) 797–826.

[14] C. Miehe, M. Hofacker, F. Welschinger, A phase field model for rate-independent crack propagation: Robust algorithmic implementation based on operator splits, Computer Methods in Applied Mechanics and Engineering 199 (45-48) (2010) 2765–2778.

[15] M. J. Borden, C. V. Verhoosel, M. A. Scott, T. J. Hughes, C. M. Landis, A phase-field description of dynamic brittle fracture, Computer Methods in Applied Mechanics and Engineering 217 (2012) 77–95.

[16] M. Ambati, T. Gerasimov, L. De Lorenzis, A review on phase-field models of brittle fracture and a new fast hybrid formulation, Computational Mechanics 55 (2) (2015) 383–405.

[17] C. Miehe, M. Hofacker, L.-M. Schänzel, F. Aldakheel, Phase field modeling of fracture in multi-physics problems. part ii. coupled brittle-to-ductile failure criteria and crack propagation in thermo-elastic–plastic solids, Computer Methods in Applied Mechanics and Engineering 294 (2015) 486–522.

[18] M. J. Borden, T. J. Hughes, C. M. Landis, A. Anvari, I. J. Lee, A phase-field formulation for fracture in ductile materials: Finite deformation balance law derivation, plastic degradation, and stress triaxiality effects, Computer Methods in Applied Mechanics and Engineering 312 (2016) 130–166.

[19] J. Choo, W. Sun, Coupled phase-field and plasticity modeling of geological materials: From brittle fracture to ductile flow, Computer Methods in Applied Mechanics and Engineering 330 (2018) 1–32.

[20] J. Fang, C. Wu, J. Li, Q. Liu, C. Wu, G. Sun, L. Qing, Phase field fracture in elasto-plastic solids: variational formulation for multi-surface plasticity and effects of plastic yield surfaces and hardening, International Journal of Mechanical Sciences (2019).

[21] X. Zhang, S. W. Sloan, C. Vignes, D. Sheng, A modification of the phase-field model for mixed mode crack propagation in rock-like materials, Computer Methods in Applied Mechanics and Engineering 322 (2017) 123–136.

[22] E. C. Bryant, W. Sun, A mixed-mode phase field fracture model in anisotropic rocks with consistent kinematics, Computer Methods in Applied Mechanics and Engineering 342 (2018) 561–584.

[23] T.-T. Nguyen, J. Rethore, J. Yvonnet, M.-C. Baietto, Multi-phase-field modeling of anisotropic crack propagation for polycrystalline materials, Computational Mechanics 60 (2) (2017) 289–314.

[24] J. Bleyer, R. Alessi, Phase-field modeling of anisotropic brittle fracture including several damage mechanisms, Computer Methods in Applied Mechanics and Engineering 336 (2018) 213–236.

[25] B. Evans, J. T. Fredrich, T.-F. Wong, The brittle-ductile transition in rocks: Recent experimental and theoretical progress, The Brittle-Ductile Transition in Rocks, Geophys. Monogr. Ser 56 (1990) 1–20.

[26] T.-f. Wong, P. Baud, The brittle-ductile transition in porous rock: A review, Journal of Structural Geology 44 (2012) 25–53.

[27] S. Zhou, X. Zhuang, T. Rabczuk, Phase field modeling of brittle compressive-shear fractures in rock-like materials: A new driving force and a hybrid formulation, Computer Methods in Applied Mechanics and Engineering 355 (2019) 729–752.

[28] F. Fei, J. Choo, A phase-field method for modeling cracks with frictional contact, International Journal for Numerical Methods in Engineering 121 (4) (2020) 740–762.

[29] A. Palmer, J. Rice, The growth of slip surfaces in the progressive failure of over-consolidated clay, Proceedings of the Royal Society of London. A. Mathematical and Physical Sciences 332 (1591) (1973) 527–548.

[30] F. Fei, J. Choo, A phase-field model of frictional shear fracture in geologic materials, Computer Methods in Applied Mechanics and Engineering 369 (2020) 113265.

[31] L. Wang, C. Vuik, H. Hajibeygi, A stabilized mixed-fe scheme for frictional contact and shear failure analyses in deformable fractured media, Engineering Fracture Mechanics 267 (2022) 108427.

[32] A. Spetz, R. Denzer, E. Tudisco, O. Dahlblom, A modified phase-field fracture model for simulation of mixed mode brittle fractures and compressive cracks in porous rock, Rock Mechanics and Rock Engineering 54 (2021) 1–14.

[33] Q. Wang, Y. Feng, W. Zhou, Y. Cheng, G. Ma, A phase-field model for mixed-mode fracture based on a unified tensile fracture criterion, Computer Methods in Applied Mechanics and Engineering 370 (2020) 113270.

[34] J. Ulloa, J. Wambacq, R. Alessi, E. Samaniego, G. Degrande, S. François, A micromechanics-based variational phase-field model for fracture in geomaterials with brittle-tensile and compressive-ductile behavior, Journal of the Mechanics and Physics of Solids 159 (2022) 104684.

[35] T. You, H. Waisman, Q.-Z. Zhu, Brittle-ductile failure transition in geomaterials modeled by a modified phase-field method with a varying damage-driving energy coefficient, International Journal of Plasticity 136 (2021) 102836.

[36] K. Oshima, T. Takaki, M. Muramatsu, Development of multi-phase-field crack model for crack propagation in polycrystal, International Journal of Computational Materials Science and Engineering 03 (2014) 1450009.

[37] T.-T. Nguyen, J. Réthoré, J. Yvonnet, M.-C. Baietto, Multi-phase-field modeling of anisotropic crack propagation for polycrystalline materials, Computational Mechanics 60 (2017) 289–314.

[38] S. Na, W. Sun, Computational thermomechanics of crystalline rock, part i: A combined multi-phase-field/crystal plasticity approach for single crystal simulations, Computer Methods in Applied Mechanics and Engineering 338 (2018) 657–691.

[39] A. Dean, P. Asur Vijaya Kumar, J. Reinoso, C. Gerendt, M. Paggi, E. Mahdi, R. Rolfes, A multi phase-field fracture model for long fiber reinforced composites based on the puck theory of failure, Composite Structures 251 (2020) 112446.

[40] J. Bleyer, R. Alessi, Phase-field modeling of anisotropic brittle fracture including several damage mechanisms, Computer Methods in Applied Mechanics and Engineering 336 (2018) 213–236.

[41] Z. Yu, J. F. Shao, M. N. Vu, G. Armand, Numerical study of thermo-hydro-mechanical responses of in situ heating test with phase-field model., International Journal of Rock Mechanics and Mining Sciences 138 (2021) 104542.

[42] F. Fei, J. Choo, Double-phase-field formulation for mixed-mode fracture in rocks, Computer Methods in Applied Mechanics and Engineering 376 (2021) 113655.

[43] T. F. Wong, Micromechanics of faulting in westerly granite, in: International journal of rock mechanics and mining sciences & geomechanics abstracts, Vol. 19, Elsevier, 1982, pp. 49–64.

[44] R. Wong, K. Chau, C. Tang, P. Lin, Analysis of crack coalescence in rock-like materials containing three flaws—part i: experimental approach, International Journal of Rock Mechanics and Mining Sciences 38 (7) (2001) 909–924.

[45] M. S. Paterson, T.-f. Wong, Experimental rock deformation-the brittle field, Springer Science & Business Media, 2005.

[46] V. Lubarda, D. Krajcinovic, S. Mastilovic, Damage model for brittle elastic solids with unequal tensile and compressive strengths, Engineering Fracture Mechanics 49 (5) (1994) 681–697.

[47] S. Murakami, Continuum damage mechanics: a continuum mechanics approach to the analysis of damage and fracture, Vol. 185, Springer Science & Business Media, 2012.

[48] C. Miehe, Comparison of two algorithms for the computation of fourth-order isotropic tensor functions, Computers & structures 66 (1) (1998) 37–43.

[49] C. Miehe, M. Lambrecht, Algorithms for computation of stresses and elasticity moduli in terms of seth–hill's family of generalized strain tensors, Communications in numerical methods in engineering 17 (5) (2001) 337–353.

[50] S. Zhang, W. Jiang, M. R. Tonks, A new phase field fracture model for brittle materials that accounts for elastic anisotropy, Computer Methods in Applied Mechanics and Engineering 358 (2020) 112643.

[51] T. T. Nguyen, J. Yvonnet, Q.-Z. Zhu, M. Bornert, C. Chateau, A phase-field method for computational modeling of interfacial damage interacting with crack propagation in realistic microstructures obtained by microtomography, Computer Methods in Applied Mechanics and Engineering 312 (2016) 567–595.

[52] J. Y. Wu, V. P. Nguyen, C. T. Nguyen, D. Sutula, S. Bordas, S. Sinaie, B. S. P. A, Chapiter one - phase field modeling of fracture, Advances in Applied Mechancis 53 (2020) 1–183.

[53] Z. Li, Q.-h. Zhu, B.-l. Tian, T.-f. Sun, D.-w. Yang, A damage model for hard rock under stress-induced failure mode, in: Advanced Engineering and Technology III: Proceedings of the 3rd Annual Congress on Advanced Engineering and Technology (CAET 2016), Hong Kong, 22-23 October 2016, CRC Press, 2017, p. 87.

[54] C. Miehe, F. Welschinger, M. Hofacker, Thermodynamically consistent phase-field models of fracture: variational principles and multi-field fe implementations, International Journal for Numerical Methods

in Engineering 83 (10) (2010) 1273–1311.

[55] B. Bourdin, G. A. Francfort, J.-J. Marigo, The variational approach to fracture, Journal of elasticity 91 (1-3) (2008) 5–148.

[56] A. Bobet, Fracture coalescence in rock materials: Experimental observations and numerical predictions., Ph.D. thesis, Massachusetts Institute of Technology (1998).

[57] A. Bobet, H. H. Einstein, Numerical modeling of fracture coalescence in a model rock material, International Journal of Fracture 92 (3) (1998) 221.

[58] H. Amor, J.-J. Marigo, C. Maurini, Regularized formulation of the variational brittle fracture with unilateral contact: Numerical experiments, Journal of the Mechanics and Physics of Solids 57 (8) (2009) 1209–1229.